Joint Pilot-Based Localization and Channel Estimation in RIS-Aided Communication Systems

Doğa Gürgünoğlu, *Student Member, IEEE*, Emil Björnson, *Fellow, IEEE*, Gabor Fodor, *Senior Member, IEEE*

***Abstract*—In this letter, we investigate the use of reconfigurable intelligent surfaces (RISs) to jointly estimate the position and channel of a user equipment (UE) using uplink pilot signals. We consider a setup with a user and a base station (BS), where the direct path between the BS and the UE is blocked and virtual line-of-sight (LOS) links are created over two reconfigurable intelligent surfaces (RISs). We investigate the benefits of exploiting the channel geometry to estimate the user's position and the user-RIS channels jointly in terms of estimation performance and pilot overhead. To this end, we consider the Cramér-Rao Lower Bound for channel estimation and UE localization. Our numerical results show that exploiting the LOS structure of the channels improves the channel estimation performance by several orders of magnitude and reduces the channel estimation performance by reducing the number of unknown parameters.**

***Index Terms*—Channel estimation, Pilot contamination, Localization, Reconfigurable intelligent surface.**

I. Introduction

The rapid advancements of wireless communication systems have been driven by the ever-increasing demand for throughput, coverage, and reliability due to social habits altered by advancing technology. As a result, the current demands for the sixth generation of wireless communication systems (6G) require a set of key enabling technologies, one of which is reconfigurable intelligent surface (RIS) [1]. An RIS is a passive device consisting of multiple metamaterial-based elements whose reflective properties are externally controllable, which allows a partial manipulation of the propagation environment in favor of communicating user equipments (UEs) [2], [3].

As 6G is designed as a multi-functional system offering massive connectivity, localization, and sensing services [4], there exists a multitude of studies considering RIS-aided localization systems and their synergies with communication systems. In [5], RIS-aided localization and sensing are discussed from a signal processing perspective. It is discussed that the RIS acts not only as an additional anchor node for localization but also as an entity boosting the system performance via configuration optimization. In [6], an RIS-aided near-field localization system is considered under phase-dependent amplitude variations of the RIS elements. In [7], RIS-aided localization is considered when some of the RIS elements fail with a certain probability. Such hardware impairments significantly affect localization performance since the system extracts sensitive geometric information from the observations to obtain the user location. On the other hand, for pure communication purposes, the unstructured channel estimates usually suffice. Nevertheless, localization information has the potential to boost communication performance significantly since the user location implicitly provides a significant portion of the channel state information (CSI), especially in line of sight (LOS)-dominant channels. To utilize this potential, synergies between localization and communication are investigated throughout the literature.

In [8], a strategy to optimize the RIS for localization and sensing is proposed.. Additionally, a user tracking scheme is also proposed in this study. In [9], position estimates are used for channel estimation. In [10], location information is used to aid the communication system by estimating angle of departure (AoD)s from Rician channel estimates.

For LOS channels in particular, there are direct relations between the geometric parameters and the channel coefficients, therefore, it is rather straightforward to estimate the channel based on the information obtained from localization. However, these relations are highly nonlinear, therefore, the achievable estimation performance is highly dependent on the values of the parameters. Therefore, theoretical analysis of the achievable estimation performance is necessary for all possible values of the parameters. To this end, we consider the uplink of a two-RIS indoor communication system, where the base station (BS) localizes a single UE and estimates its channel based on the location estimate. The BS utilizes the same set of pilot transmissions for both tasks by estimating the channel gain, propagation delay, and angle of arrivals (AoAs) of the signals impinging on both RISs, and using the RIS and system geometry to estimate the channel and the UE position. As our performance metric for location and channel estimation, we consider the Cramér-Rao Lower Bound (CRLB), which provides a lower bound on the variance of any unbiased estimator. In addition, we consider the use of parameter estimates for channel estimation as a potential solution for the additional pilot overhead caused by using multiple RISs demonstrated in [11]. Our contributions in this letter can be summarized as follows:

- For both channel estimation and user localization, we provide the CRLB on the mean squared error (MSE) in closed form for all user locations.
- In the presence of multiple RISs, we show that parametric channel estimation yields more accurate channel estimates with fewer pilot transmissions than non-parametric channel estimation. We demonstrate this by comparing the CRLBs on parametric and non-parametric channel estimation MSEs, where the non-parametric estimation

Doğa Gürgünoğlu and Gabor Fodor are with the Division of Decision and Control Systems at KTH Royal Institute of Technology, 100 44 Stockholm, Sweden, and Ericsson Research, Stockholm 164 80, Sweden. Emil Björnson is with the Division of Communication Systems at KTH Royal Institute of Technology, 100 44 Stockholm, Sweden. This study is supported by EU Horizon 2020 MSCA-ITN-METAWIRELESS, Grant Agreement 956256. E. Björnson is supported by the FFL18-0277 grant from the Swedish Foundation for Strategic Research. G. Fodor was partially funded by the 6G-MUSICAL project.

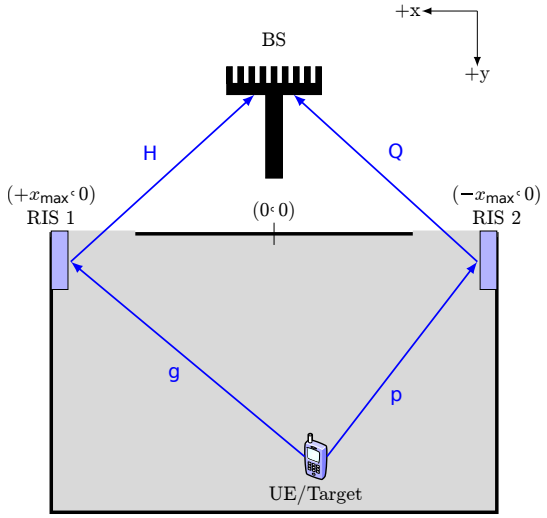

Fig. 1: Two-RIS localization system. The coordinate system within the room is specified with the axis arrows in the upper right corner of the figure, and the origin of the coordinate system corresponds to the point marked in the middle of the two side walls on which the RISs are mounted on, and on the receiver-side wall. The room is $2x_{\max}$ meters wide, that is, RIS 1 and RIS 2 are located at the coordinates $(+x_{\max}, 0)$ and $(-x_{\max}, 0)$ respectively. The room extends down the y-axis up to $y_{\max}$ meters, i.e., the rear corners correspond to $(+x_{\max}, +y_{\max})$ and $(-x_{\max}, +y_{\max})$.

scheme uses twice as many pilots as the parametric estimation scheme does.

II. System Model

We consider the indoor joint communication and localization setup aided by two RISs illustrated in Fig. 1. The matrices $\mathbf{H} \in \mathbb{C}^{M\times N}$ and $\mathbf{Q} \in \mathbb{C}^{M\times N}$ denote the static and known channels between the RISs and the M-antenna BS, where N is the number of elements in each RIS. Moreover, the channels between the unknown target/UE to the RISs, assumed to be purely LOS, are denoted by $\mathbf{g} \in \mathbb{C}^N$ and $\mathbf{p} \in \mathbb{C}^N$. The signal received after a single pilot transmission can be expressed as

$$\mathbf{y}_p = \sqrt{P_p}(\mathbf{H}\boldsymbol{\Phi}_1\mathbf{g} + \mathbf{Q}\boldsymbol{\Phi}_2\mathbf{p})s + \mathbf{w} \in \mathbb{C}^{M\times 1}, \quad (1)$$

where P_p denotes the pilot transmission power, $\boldsymbol{\Phi}_k = \text{Diag}(e^{-j\phi_{k1}}, \ldots, e^{-j\phi_{kN}}) \in \mathbb{C}^{N\times N}$ denotes the diagonal response matrix of RIS k, $s \in \mathbb{C}$ denotes the transmitted positioning reference signal, and $\mathbf{w} \sim \mathcal{CN}(\mathbf{0}, \sigma_w^2\mathbf{I}_M)$ denotes the additive receiver noise. When considering the estimation of channel-related parameters, it is more convenient to rewrite (1) as

$$\mathbf{y}_p = \sqrt{P_p}(\boldsymbol{\phi}_1\mathbf{D}_\mathbf{H}\mathbf{g} + \boldsymbol{\phi}_2\mathbf{D}_\mathbf{Q}\mathbf{p})s + \mathbf{w} \in \mathbb{C}^{M\times 1}, \quad (2)$$

where $\mathbf{D}_\mathbf{H} \triangleq \text{Diag}(\mathbf{H}_1, \ldots, \mathbf{H}_N) \in \mathbb{C}^{MN\times N}$, $\mathbf{D}_\mathbf{Q} \triangleq \text{Diag}(\mathbf{Q}_1, \ldots, \mathbf{Q}_N) \in \mathbb{C}^{MN\times N}$ with $\mathbf{H}_n$ and $\mathbf{Q}_n$ denoting the n-th columns of $\mathbf{H}$ and $\mathbf{Q}$, respectively, and $\boldsymbol{\phi}_k = \text{diag}(\boldsymbol{\Phi}_k) \otimes \mathbf{I}_M \in \mathbb{C}^{MN\times M}$ for $k = 1, 2$. $\mathbf{D}_\mathbf{H}$ and $\mathbf{D}_\mathbf{Q}$ are block diagonal matrices built of $M \times 1$ blocks, and the diagonal blocks contain the individual columns of $\mathbf{H}$ and $\mathbf{Q}$. Assuming that the pilot transmission is repeated over time $L \geq N$ times with varying RIS configurations and $s[l] = 1$ for $l = 1, \ldots, L$, we can express the collection of observations $\mathbf{Y}_p \triangleq [\mathbf{y}_p^T[1], \ldots, \mathbf{y}_p^T[L]]^T$ as

$$\mathbf{Y}_p = \sqrt{P_p}(\mathbf{B}_1\mathbf{D}_\mathbf{H}\mathbf{g} + \mathbf{B}_2\mathbf{D}_\mathbf{Q}\mathbf{p}) + \mathbf{W} \in \mathbb{C}^{LM}, \quad (3)$$

where $\mathbf{B}_k \triangleq [\boldsymbol{\phi}_k[1], \ldots, \boldsymbol{\phi}_k[L]]^T \in \mathbb{C}^{LM\times MN}$ and $\mathbf{W} \sim \mathcal{CN}(\mathbf{0}, \sigma_w^2\mathbf{I}_{LM})$. Note that $\phi_k[l]$ also contains the pilot signals $s[l]$, however, since we choose $s[l] = 1$ for $l = 1, \ldots, L$, $\phi_k[l]$ are the same as the RIS configurations.

Since we consider purely LOS channels, the unknown $\mathbf{g}$ and $\mathbf{p}$ channels are structured based on the RIS geometries, attenuation, and propagation delay. For both RISs, we consider the uniform linear array (ULA) geometry and perform 2D localization in the far-field region. Based on the azimuth AoAs φ_1 and φ_2 on RIS 1 and RIS 2, respectively, $\mathbf{g}$ and $\mathbf{p}$ can be expressed as

$$\mathbf{g} = \sqrt{\alpha_1}e^{-j2\pi f_c\tau_1}\mathbf{a}(\varphi_1), \quad (4a)$$

$$\mathbf{p} = \sqrt{\alpha_2}e^{-j2\pi f_c\tau_2}\mathbf{a}(\varphi_2), \quad (4b)$$

where $\mathbf{a}(\varphi) = \begin{bmatrix}1 & e^{-j2\pi\frac{\Delta}{\lambda}\sin(\varphi)} & \ldots & e^{-j2\pi(N-1)\frac{\Delta}{\lambda}\sin(\varphi)}\end{bmatrix}^T$ denotes the array steering vector for the ULA geometry. In the next section, we derive the CRLB on the channel estimation MSE and the UE localization error.

III. CRLB on Localization and Channel Estimation

In a parameter estimation problem, it is useful to determine an achievable lower bound on the estimation performance to serve as the gold standard. The CRLB—the inverse of the Fisher Information Matrix (FIM)—provides a lower bound on the MSE of any unbiased estimator [12] via the following matrix inequality:

$$\text{Cov}(\hat{\boldsymbol{\theta}}(\mathbf{X})) \succeq \mathbf{I}^{-1}(\mathbf{X}; \boldsymbol{\theta}) \quad (5)$$

for an estimate of a parameter vector $\boldsymbol{\theta}$ based on an observation vector $\mathbf{X}$. Here, $\text{Cov}(\hat{\boldsymbol{\theta}}(\mathbf{X})) = \mathbb{E}[(\hat{\boldsymbol{\theta}}(\mathbf{X})-\boldsymbol{\theta})(\hat{\boldsymbol{\theta}}(\mathbf{X})-\boldsymbol{\theta})^H]$ is the covariance matrix and, consequently, the bound on the sum MSE can be expressed as

$$\mathbb{E}[\|\hat{\boldsymbol{\theta}}(\mathbf{X}) - \boldsymbol{\theta}\|^2] \geq \text{tr}\left(\mathbf{I}^{-1}(\mathbf{X}; \boldsymbol{\theta})\right). \quad (6)$$

In a generic vector parameter estimation problem, the FIM is computed via the following equation [13, Eq. 3.21]:

$$[\mathbf{I}(\mathbf{X}; \boldsymbol{\theta})]_{ij} = -\mathbb{E}\left[\frac{\partial^2 \ln(f(\mathbf{X}; \boldsymbol{\theta}))}{\partial\theta_i\theta_j}\right], \quad (7)$$

where $f(\mathbf{X}; \boldsymbol{\theta})$ denotes the likelihood function of the observation $\mathbf{X}$ based on the unknown vector parameter $\boldsymbol{\theta}$. In our channel estimation problem, the received pilot signal in (3) can be expressed as

$$\mathbf{Y}_p = \sqrt{P_p}\underbrace{\begin{bmatrix}\mathbf{B}_1\mathbf{D}_\mathbf{H} & \mathbf{B}_2\mathbf{D}_\mathbf{Q}\end{bmatrix}}_{\triangleq\mathbf{F}}\underbrace{\begin{bmatrix}\mathbf{g}\\ \mathbf{p}\end{bmatrix}}_{\triangleq\mathbf{v}} + \mathbf{W}. \quad (8)$$

Here, $\mathbf{v}$ denotes the ensemble of unknown channel coefficients without any LOS parametrization. In this form, we have a linear observation model with additive complex Gaussian noise. Consequently, it is much easier to compute the FIM here than explicitly differentiating the log-likelihood function as one would do for a generic parameter-observation model. Using this special form of the observation model in (8), the FIM can be expressed as

$$\mathbf{I}(\mathbf{Y}_p; \mathbf{v}) = P_p\mathbf{F}^H\mathbf{I}(\mathbf{W})\mathbf{F}, \quad (9)$$

where $\mathbf{I}(\mathbf{W})$ denotes the FIM with respect to a translation parameter defined in [14, Eq. 8]. Since $\mathbf{w}$ is Gaussian, it

satisfies the relation $\mathbf{I}(\mathbf{W}) \succeq \frac{1}{\sigma_w^2}\mathbf{I}$ in [14, Eq. 10] with equality. Therefore, (9) can be simplified as

$$\mathbf{I}(\mathbf{Y}_p;\mathbf{v}) = \frac{P_p}{\sigma_w^2}\mathbf{F}^H\mathbf{F} \in \mathbb{C}^{2N\times 2N}. \tag{10}$$

The rank of (10) depends on the column rank of $\mathbf{F}$, which depends on the choice of $\mathbf{B}_1$ and $\mathbf{B}_2$. To ensure that the FIM is non-singular, one must have $L \geq 2N$, and $\mathbf{F}$ must have full column rank. To this end, it is tempting to choose $\mathbf{B}_1$ and $\mathbf{B}_2$ such that $\mathbf{B}_1^H\mathbf{B}_2 = \mathbf{0}$ as this configuration allows the pilot signals to explore all the unknown dimensions of the channel. When the channels $\mathbf{g}_k$ and $\mathbf{p}_k$ do not exhibit any structure, this method provides accurate channel estimates, as shown in [11]. For the non-parametric channel estimation problem, the signal model is as in (8), and the maximum likelihood (ML) estimate of $\mathbf{v}$ can be expressed as

$$\hat{\mathbf{v}} = \frac{1}{\sqrt{P_p}}(\mathbf{F}^H\mathbf{F})^{-1}\mathbf{F}^H\mathbf{y}_p. \tag{11}$$

For (11) to exist, $\mathbf{F}^H\mathbf{F}$ should be invertible, which is maintained by choosing $\mathbf{B}_1^H\mathbf{B}_2 = \mathbf{0}$. This also implies that the FIM is invertible, that is the CRLB exists and can be expressed as

$$\mathbf{I}^{-1}(\mathbf{Y}_p;\mathbf{v}) = \frac{\sigma_w^2}{P_p}(\mathbf{F}^H\mathbf{F})^{-1}. \tag{12}$$

On the other hand, the error covariance matrix achieved by (11) becomes

$$\begin{aligned}
&\mathbb{E}[(\hat{\mathbf{v}}-\mathbf{v})(\hat{\mathbf{v}}-\mathbf{v})^H] = \mathbb{E}[\hat{\mathbf{v}}\hat{\mathbf{v}}^H] + \mathbf{v}\mathbf{v}^H - 2\mathrm{Re}\{\mathbb{E}[\hat{\mathbf{v}}\mathbf{v}^H]\}\\
&= \frac{1}{P_p}(\mathbf{F}^H\mathbf{F})^{-1}\mathbf{F}^H\mathbb{E}[\mathbf{y}_p\mathbf{y}_p^H]\mathbf{F}(\mathbf{F}^H\mathbf{F})^{-1}\\
&+ \mathbf{v}\mathbf{v}^H - 2\mathrm{Re}\left\{\frac{1}{\sqrt{P_p}}(\mathbf{F}^H\mathbf{F})^{-1}\mathbf{F}^H\mathbb{E}[\mathbf{y}_p\mathbf{v}^H]\right\}\\
&= \mathbf{v}\mathbf{v}^H + \frac{\sigma_w^2}{P_p}(\mathbf{F}^H\mathbf{F})^{-1} + \mathbf{v}\mathbf{v}^H - 2\mathbf{v}\mathbf{v}^H = \frac{\sigma_w^2}{P_p}(\mathbf{F}^H\mathbf{F})^{-1},
\end{aligned} \tag{13}$$

which shows that $\hat{\mathbf{v}}$ achieves the CRLB when $\mathbf{F}^H\mathbf{F}$ is full-rank. While this estimator works successfully when the channels of interest do not exhibit any structure, the minimum number of pilots required increases significantly with an increasing number of RIS elements.

A. CRLB on UE Localization Error

So far, we have derived the FIM between the observation $\mathbf{y}_p$ and the channel coefficients $\mathbf{v}$ when the UE-RIS channels do not exhibit any structure. When these channels have parametric LOS structures, however, they can be expressed in terms of much fewer parameters, as in (4), which is quite convenient in terms of reducing the number of pilot transmissions since the number of RIS elements N can be very large in practice. To overcome this, we can exploit our knowledge of the RISs' geometry since each N-dimensional channel can be expressed in terms of three parameters: attenuation, propagation delay, and azimuth angle of arrival While α_k, τ_k, and φ_k seem like independent parameters, they are coupled through the UE position $\mathbf{z} \triangleq \begin{bmatrix} x_t & y_t \end{bmatrix}^T$. While the propagation delays' and azimuth AoAs' relations with the UE are straightforward, we can use the free space path loss model to relate the attenuation parameters to (x_t, y_t) as follows:

$$\alpha_1 = \left(\frac{c}{4\pi f_c\sqrt{y_t^2 + (x_{\max}-x_t)^2}}\right)^2 \tag{14a}$$

$$\alpha_2 = \left(\frac{c}{4\pi f_c\sqrt{y_t^2 + (x_{\max}+x_t)^2}}\right)^2 \tag{14b}$$

$$\tau_1 = \frac{\sqrt{y_t^2 + (x_{\max}-x_t)^2}}{c} \tag{14c}$$

$$\tau_2 = \frac{\sqrt{y_t^2 + (x_{\max}+x_t)^2}}{c} \tag{14d}$$

$$\varphi_1 = \tan^{-1}\left(\frac{y_t}{x_{\max}-x_t}\right) \tag{14e}$$

$$\varphi_2 = \tan^{-1}\left(\frac{y_t}{x_{\max}+x_t}\right) \tag{14f}$$

By combining (4) and (14), we can define the following non-linear transformation between the UE coordinates and the channels to be estimated as $\boldsymbol{\beta}(\mathbf{z}) \triangleq \mathbf{v}$.

To obtain the FIM between $\mathbf{Y}_p$ and $\mathbf{z}$, we need to use a well-known result [13, Eq. 3.30]:

$$\mathbf{I}^{-1}(\mathbf{Y}_p;\boldsymbol{\beta}(\mathbf{z})) = \mathbf{J}_{\boldsymbol{\beta}}^H\mathbf{I}^{-1}(\mathbf{Y}_p;\mathbf{z})\mathbf{J}_{\boldsymbol{\beta}}, \tag{15}$$

where $\mathbf{J}_{\boldsymbol{\beta}}$ is the Jacobian of $\boldsymbol{\beta}$ w.r.t. $\mathbf{z}$, which is a $2\times 2N$ matrix where the ijth entry is $[\mathbf{J}_{\boldsymbol{\beta}}]_{ij} = \frac{\partial\beta_j(\mathbf{z})}{\partial z_i}$. Using the Moore-Penrose pseudoinverse of the Jacobian, one can obtain $\mathbf{I}^{-1}(\mathbf{Y}_p;\mathbf{z})$ as

$$\mathbf{I}^{-1}(\mathbf{Y}_p;\mathbf{z}) = (\mathbf{J}_{\boldsymbol{\beta}}\mathbf{J}_{\boldsymbol{\beta}}^H)^{-1}\mathbf{J}_{\boldsymbol{\beta}}\mathbf{I}^{-1}(\mathbf{Y}_p;\boldsymbol{\beta}(\mathbf{z}))\mathbf{J}_{\boldsymbol{\beta}}^H(\mathbf{J}_{\boldsymbol{\beta}}\mathbf{J}_{\boldsymbol{\beta}}^H)^{-1}. \tag{16}$$

To obtain $\mathbf{I}^{-1}(\mathbf{Y}_p;\mathbf{z})$ in closed form, what remains is to obtain $\mathbf{J}_{\boldsymbol{\beta}}$. To this end, we can express $\mathbf{J}_{\boldsymbol{\beta}}$ as a 2×2 block matrix of $1\times N$ entries:

$$\mathbf{J}_{\boldsymbol{\beta}} = \begin{bmatrix} \frac{\partial\mathbf{g}}{\partial x_t} & \frac{\partial\mathbf{p}}{\partial x_t} \\ \frac{\partial\mathbf{g}}{\partial y_t} & \frac{\partial\mathbf{p}}{\partial y_t} \end{bmatrix} \tag{17}$$

By using the chain rule for derivatives on (4), we obtain

$$\begin{aligned}
\frac{\partial\mathbf{g}}{\partial x_t} &= e^{-j2\pi f_c\tau_1}\left[\frac{1}{2\sqrt{\alpha_1}}\frac{\partial\alpha_1}{\partial x_t}\mathbf{a}(\varphi_1)\right.\\
&\left. - j2\pi f_c\frac{\partial\tau_1}{\partial x_t}\sqrt{\alpha_1}\mathbf{a}(\varphi_1) + \sqrt{\alpha_1}\frac{\partial\mathbf{a}(\varphi_1)}{\partial\varphi_1}\frac{\partial\varphi_1}{\partial x_t}\right],
\end{aligned} \tag{18a}$$

$$\begin{aligned}
\frac{\partial\mathbf{p}}{\partial x_t} &= e^{-j2\pi f_c\tau_2}\left[\frac{1}{2\sqrt{\alpha_2}}\frac{\partial\alpha_2}{\partial x_t}\mathbf{a}(\varphi_2)\right.\\
&\left. - j2\pi f_c\frac{\partial\tau_2}{\partial x_t}\sqrt{\alpha_1}\mathbf{a}(\varphi_2) + \sqrt{\alpha_2}\frac{\partial\mathbf{a}(\varphi_2)}{\partial\varphi_2}\frac{\partial\varphi_2}{\partial x_t}\right],
\end{aligned} \tag{18b}$$

$$\begin{aligned}
\frac{\partial\mathbf{g}}{\partial y_t} &= e^{-j2\pi f_c\tau_1}\left[\frac{1}{2\sqrt{\alpha_1}}\frac{\partial\alpha_1}{\partial y_t}\mathbf{a}(\varphi_1)\right.\\
&\left. - j2\pi f_c\frac{\partial\tau_1}{\partial y_t}\sqrt{\alpha_1}\mathbf{a}(\varphi_1) + \sqrt{\alpha_1}\frac{\partial\mathbf{a}(\varphi_1)}{\partial\varphi_1}\frac{\partial\varphi_1}{\partial y_t}\right],
\end{aligned} \tag{18c}$$

$$\begin{aligned}
\frac{\partial\mathbf{p}}{\partial y_t} &= e^{-j2\pi f_c\tau_2}\left[\frac{1}{2\sqrt{\alpha_2}}\frac{\partial\alpha_2}{\partial y_t}\mathbf{a}(\varphi_2)\right.\\
&\left. - j2\pi f_c\frac{\partial\tau_2}{\partial y_t}\sqrt{\alpha_1}\mathbf{a}(\varphi_2) + \sqrt{\alpha_2}\frac{\partial\mathbf{a}(\varphi_2)}{\partial\varphi_2}\frac{\partial\varphi_2}{\partial y_t}\right],
\end{aligned} \tag{18d}$$

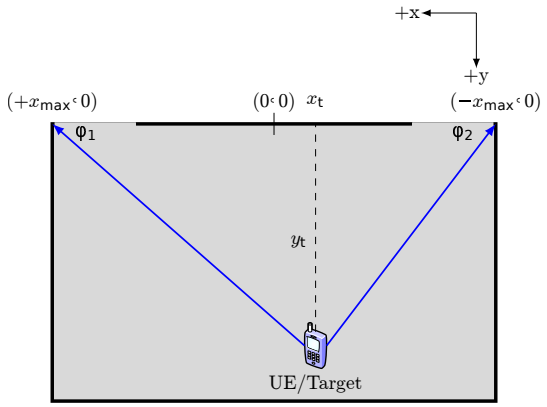

Fig. 2: The geometrical relationship between the azimuth AoAs and the cartesian coordinates.

In (18), the derivatives to be evaluated are $\frac{\partial \mathbf{a}}{\partial \varphi}$, $\frac{\partial \alpha_k}{\partial x_t}, \frac{\partial \alpha_k}{\partial y_t}$, $\frac{\partial \tau_k}{\partial x_t}, \frac{\partial \tau_k}{\partial y_t}$, $\frac{\partial \varphi_k}{\partial x_t}$, and $\frac{\partial \varphi_k}{\partial y_t}$. Using the array steering vector formula and (14), we can evaluate these as follows:

$$\frac{\partial \mathbf{a}}{\partial \varphi} = \begin{bmatrix} 0 & \dots & -j2\pi \frac{\Delta}{\lambda}(N-1)\cos(\varphi) e^{-j2\pi \frac{\Delta}{\lambda}(N-1)\sin(\varphi)} \end{bmatrix}^T \tag{19a}$$

$$\frac{\partial \alpha_k}{\partial x_t} = \frac{\pm 32\pi^2 f_c^2 c^2 (x_{\max} \mp x_t)}{\left[16\pi^2 f_c^2 (x_{\max} \mp x_t)^2 + 16\pi^2 f_c^2 y_t^2\right]^2} \tag{19b}$$

$$\frac{\partial \alpha_k}{\partial y_t} = \frac{-32\pi^2 f_c^2 c^2 y_t}{\left[16\pi^2 f_c^2 (x_{\max} \mp x_t)^2 + 16\pi^2 f_c^2 y_t^2\right]^2} \tag{19c}$$

$$\frac{\partial \tau_k}{\partial x_t} = \frac{\mp (x_{\max} \mp x_t)}{c\sqrt{(x_{\max} \mp x_t)^2 + y_t^2}} \tag{19d}$$

$$\frac{\partial \tau_k}{\partial y_t} = \frac{y_t}{c\sqrt{(x_{\max} \mp x_t)^2 + y_t^2}} \tag{19e}$$

$$\frac{\partial \varphi_k}{\partial x_t} = \frac{\mp y_t^2}{y_t^2 + (x_{\max} \mp x_t)^2} \tag{19f}$$

$$\frac{\partial \varphi_k}{\partial y_t} = \frac{(x_{\max} \mp x_t)}{y_t^2 + (x_{\max} \mp x_t)^2} \tag{19g}$$

As a result, we obtain the Jacobian in closed form and therefore have $\mathbf{I}^{-1}(\mathbf{Y}_p; \mathbf{z})$. The diagonal entries of this matrix provide a lower bound on the squared error in estimating x_t and y_t. To obtain the localization error bound (LEB) in meters, we just have to calculate the 2-norm of the resulting error vector. Consequently, the LEB becomes

$$\text{LEB} = \sqrt{\text{tr}(\mathbf{I}^{-1}(\mathbf{Y}_p; \mathbf{z}))}. \tag{20}$$

B. CRLB on Channel Estimation MSE

The inverse FIM between $\mathbf{Y}_p$ and the cartesian coordinates of the UE we derived using the channel geometry provides the goldens standard for any unbiased location estimator. Using a similar idea, we can obtain a lower bound on the performance of unbiased parametric channel estimators by using the non-linear transformation $\mathbf{v} = \boldsymbol{\beta}(\mathbf{z})$, similar to the parametric estimation idea in [15]. While we do not derive any parametric estimators in this letter, we provide the CRLB as an indicator of what is achievable if a parametric channel estimator were to be designed for such a system. To determine the CRLB on parametric channel estimation MSE, using (15) suffices, that is:

$$\text{Cov}(\boldsymbol{\beta}(\hat{\mathbf{z}})) \succeq \mathbf{J}_{\boldsymbol{\beta}}^H \mathbf{I}^{-1}(\mathbf{Y}_p; \mathbf{z}) \mathbf{J}_{\boldsymbol{\beta}}. \tag{21}$$

Parameter	Value
P_p	50 dBm
σ_w^2	-104 dBm
f_c	30 GHz
M	64
N	16
L	16, 32
$x_{\max}$	20 m
$y_{\max}$	40 m

TABLE I: System parameters used for the numerical results. The value for σ_w^2 is obtained by considering a 10 MHz transmission bandwidth and a noise power spectral density of -174dBm/Hz. In addition, the BS is located at $(10, -40)$ according to the coordinate system provided in Fig. 2.

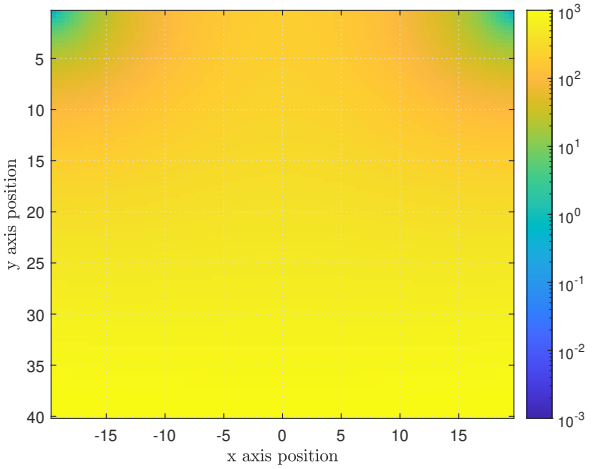

Fig. 3: Non-parametric channel estimation MSE for $\mathbf{B}_1^H \mathbf{B}_2 = \mathbf{0}$. Note that we transmit $L = 2N$ pilots for non-parametric estimation as opposed to $L = N$ pilots for parametric estimation.

IV. Numerical Results

In this section, we provide numerical examples for the analysis we have provided. To this end, we consider the set of system parameters in Table I. To capture large-scale effects, we consider the free space path loss model. Fig. 3 and 4 show the normalized channel estimation CRLB, that

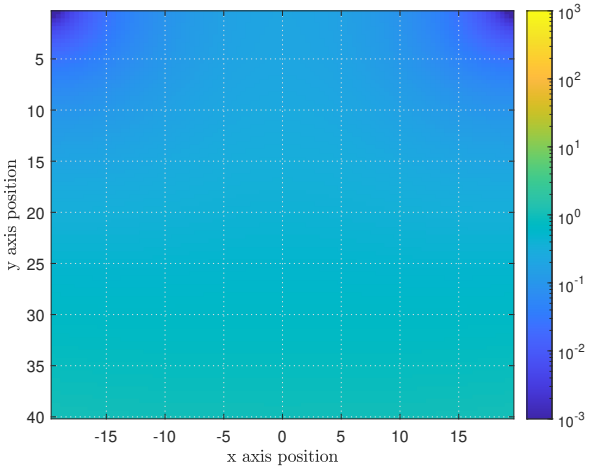

Fig. 4: CRLB on the parametric channel estimation MSE for $\mathbf{B}_1 = \mathbf{B}_2$. Note that the channel estimation MSE is decreased by three orders of magnitude compared to Fig. 3 although half as many pilots are used.

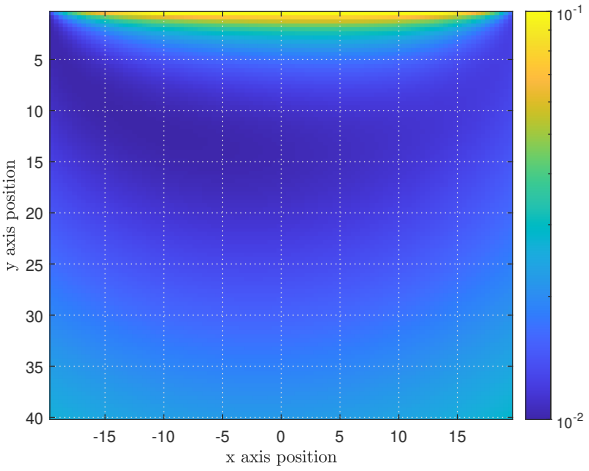

Fig. 5: CRLB on UE localization in meters. Note that the figure indicates sub-decimeter localization accuracy for the entire area, and almost centimeter-level localization accuracy around where the localization geometry is the most favorable.

is, we normalize the traces of the CRLBs in (12) and (21), respectively, by $\|\mathbf{v}\|_2^2 = 2N$. Note that parametric estimation vastly outperforms the non-parametric estimation. Although the non-parametric estimation uses twice as many pilots as the parametric estimation, the knowledge of the channel structure in parametric estimation significantly reduces the number of unknown parameters and boosts the channel estimation performance by three orders of magnitude. Non-parametric channel estimation also yields very high MSE due to the high carrier frequency and severe path loss.

In Fig. 5, we plot the LEB (in meters) throughout the room, as provided by (20). Note that for a large part of the surface of the room, the localization accuracy is at the sub-decimeter level. However, the significant inaccuracy at around $y_t = 0$ must be noted. In this region, both RISs receive the UE's signal almost perpendicularly, and hence the observation is not so sensitive to the exact position of the UE, resulting in low Fisher information. Even in this region, the accuracy is between meter and decimeter levels.

V. Conclusion

In this letter, we investigated the use of RISs for an integrated communication and localization system in an indoor environment. We proposed a setup with a single-antenna UE and an M-antenna BS between which pure LOS links are maintained via two N-element RISs. By exploiting the channel and indoor geometries, we showed that it is possible to use the same pilot signals to estimate the position of the UE, and the UE-RIS channels. As the performance metric, we used the CRLB, the lower bound on the MSE of any unbiased estimator. Through numerical examples, we showed that it is feasible to use two RISs to locate an indoor user and utilize the location information to estimate the unknown channels. Considering the parametric structures of LOS channels not only brings the benefits of reducing the pilot transmission overhead, but also improves the channel estimation performance by multiple orders of magnitude and hence acts as a precursor to a plethora of possibilities in localization-aided channel estimation to develop more pilot-efficient systems. In this letter, we considered the estimation of pure-LOS channels exploiting the channel structure, which is quite significant due to the more structured nature of mmWave channels compared to the channels with μ-wave frequencies [16]. While our analysis is extendable to scenarios with a direct UE-BS path, we considered a setup where the direct path is blocked in this work, which is realistic at mmWave/THz frequencies due to high penetration losses. Although we ignored the presence of scattering clusters, the analysis provided in this paper is extendable to clustered channel models, which will be investigated in future work.

References

[1] C. Pan, H. Ren, K. Wang, J. F. Kolb, M. Elkashlan, M. Chen, M. Di Renzo, Y. Hao, J. Wang, A. L. Swindlehurst, X. You, and L. Hanzo, "Reconfigurable intelligent surfaces for 6G systems: Principles, applications, and research directions," *IEEE Communications Magazine*, vol. 59, no. 6, pp. 14–20, 2021.

[2] E. Björnson, Ö. Özdogan, and E. G. Larsson, "Reconfigurable intelligent surfaces: Three myths and two critical questions," *IEEE Commun. Mag.*, no. 12, pp. 90–96, 2020.

[3] G. T. de Arajo, A. L. F. de Almeida, R. Boyer, and G. Fodor, "Semi-blind joint channel and symbol estimation for irs-assisted mimo systems," *IEEE Transactions on Signal Processing*, vol. 71, pp. 1184–1199, 2023.

[4] C.-X. Wang, X. You, X. Gao, X. Zhu, Z. Li, C. Zhang, H. Wang, Y. Huang, Y. Chen, H. Haas, J. S. Thompson, E. G. Larsson, M. D. Renzo, W. Tong, P. Zhu, X. Shen, H. V. Poor, and L. Hanzo, "On the road to 6g: Visions, requirements, key technologies, and testbeds," *IEEE Communications Surveys & Tutorials*, vol. 25, no. 2, pp. 905–974, 2023.

[5] E. Bjrnson, H. Wymeersch, B. Matthiesen, P. Popovski, L. Sanguinetti, and E. de Carvalho, "Reconfigurable intelligent surfaces: A signal processing perspective with wireless applications," *IEEE Signal Processing Magazine*, vol. 39, no. 2, pp. 135–158, 2022.

[6] C. Ozturk, M. F. Keskin, H. Wymeersch, and S. Gezici, "RIS-aided near-field localization under phase-dependent amplitude variations," *IEEE Transactions on Wireless Communications*, vol. 22, no. 8, pp. 5550–5566, 2023.

[7] C. Ozturk, M. F. Keskin, V. Sciancalepore, H. Wymeersch, and S. Gezici, "Ris-aided localization under pixel failures," *IEEE Transactions on Wireless Communications*, pp. 1–1, 2024.

[8] S. Palmucci, A. Guerra, A. Abrardo, and D. Dardari, "Two-timescale joint precoding design and RIS optimization for user tracking in near-field MIMO systems," *IEEE Transactions on Signal Processing*, vol. 71, pp. 3067–3082, 2023.

[9] F. Jiang, A. Abrardo, K. Keykhosravi, H. Wymeersch, D. Dardari, and M. Di Renzo, "Two-timescale transmission design and ris optimization for integrated localization and communications," *IEEE Transactions on Wireless Communications*, vol. 22, no. 12, pp. 8587–8602, 2023.

[10] X. Hu, C. Zhong, Y. Zhang, X. Chen, and Z. Zhang, "Location information aided multiple intelligent reflecting surface systems," *IEEE Transactions on Communications*, vol. 68, no. 12, pp. 7948–7962, 2020.

[11] D. Gürgünoğlu, E. Björnson, and G. Fodor, "Combating inter-operator pilot contamination in reconfigurable intelligent surfaces assisted multi-operator networks," *IEEE Transactions on Communications*, pp. 1–1, 2024.

[12] H. V. Poor, *An Introduction to Signal Detection and Estimation (2nd Ed.)*. Berlin, Heidelberg: Springer-Verlag, 1994.

[13] S. M. Kay, *Fundamentals of Statistical Signal Processing, Volume I: Estimation Theory*. Prentice Hall, 1993.

[14] R. Zamir, "A proof of the Fisher information inequality via a data processing argument," *IEEE Transactions on Information Theory*, vol. 44, no. 3, pp. 1246–1250, 1998.

[15] E. Björnson and P. Ramezani, "Maximum likelihood channel estimation for RIS-aided communications with LOS channels," in *Asilomar Conference on Signals, Systems and Computers*, 2022.

[16] S. Buzzi and C. D'Andrea, "Massive mimo 5g cellular networks: mm-wave vs. -wave frequencies," *ZTE Communications*, vol. 15 (S1), pp. 41–49, 2017.